Electronic structure and wave functions of interface states in HgTe-CdTe quantum wells and superlattices

M. Fornari
Dipartimento di Fisica Teorica, Università di Trieste and Istituto Nazionale di Fisica della Materia, Strada Costiera No. 11, I-34014 Trieste, Italy

H. H. Chen and L. Fu
Department of Physics, The Catholic University of America, Washington, D.C. 20064

R. D. Graft
U.S. Army Research Laboratory, Infrared Technology Branch, Fort Belvoir, Virginia 22060

D. J. Lohrmann
U.S. Army Center for Night-Vision and Electro-Optics, Fort Belvoir, Virginia 22060

S. Moroni
International Center for Theoretical Physics, Strada Costiera No. 11, I-34014 Trieste, Italy

G. Pastori Parravicini
Dipartimento di Fisica ''A. Volta,'' Università di Pavia and Istituto Nazionale di Fisica della Materia, Via Bassi No. 6, 27100 Pavia, Italy

L. Resca
Department of Physics, The Catholic University of America, Washington, D.C. 20064

M. A. Stroscio
U.S. Army Research Office, P.O. Box 12211 Research Triangle Park, North Carolina 27709-2211
(Received 19 August 1996; revised manuscript received 7 November 1996)

We report on extensive tight-binding calculations of electronic states in HgTe-CdTe heterojunctions, quantum wells, and superlattices. The method of solution is based on the Green's function and a powerful renormalization technique. While the band structures that we obtain are basically consistent with previous calculations by other authors with several different methods and parametrizations, we have made substantial progress in the detailed study of the corresponding wave functions and their atomic-orbital content. That allows a conclusive identification and analysis of the peculiar interface states that occur in these microstructures, and shows the crucial role played by the s-p mixing that derives from coupling of Γ_8- and Γ_6-like bands of the composing materials. In particular, the critical concentration x_a at which the semimetal-semiconductor transition occurs in the $Hg_{1-x}Cd_xTe$ simple alloy is shown to be related to a critical concentration x_c occurring in $(HgTe)_m(Hg_{1-x}Cd_xTe)_n$ superlattice alloys, at which interfacial states (anti)cross, with maximum s-p mixing. We also apply a modified (two- or n-step) Lanczos method to determine real and imaginary parts of all the components of the wave-function *amplitude*, to confirm or further investigate the complete nodal structure. Finally, we present some results regarding the question of large versus small valence-band offset for this type of interface. [S0163-1829(97)08224-6]

I. INTRODUCTION

A considerable effort to understand the peculiar behavior of HgTe-CdTe superlattices (SL's) has produced in the last two decades a great deal of good results. Experimental investigations have included most noticeably absorption,[1] photoluminescence,[2] magnetooptical, and magnetotransport measurements.[3] Theoretical studies have been based on the effective-mass approximation and $\mathbf{k}\cdot\mathbf{p}$ methods,[2,4] as well as tight-binding (TB) schemes.[5] This has allowed a fairly consistent interpretation and understanding of a broad range of properties of these microstructures.

In particular, it has been conclusively established that $(HgTe)_m(CdTe)_n$ SL's exhibit three different regimes.[2,6] Indeed, our calculations confirm that $(HgTe)_m(CdTe)_8$, for example, is a semiconductor for $m \lesssim 20$, a semimetal for $20 \lesssim m \lesssim 28$, and an inverted-gap semiconductor for $m \gtrsim 28$. Such behavior is a consequence of the peculiar inverted band structure of HgTe. An interesting relationship with an analogous behavior in the $Hg_{1-x}Cd_xTe$ alloy has also been investigated.[7] In the alloy, the semimetallic $\rightarrow$ semiconductor transition occurs around $x_a = 0.16$: our investigation quantitatively confirms and explains the connection with the superlattice regimes, as we will show.

The issue of the valence-band offset (VBO), which bears on several experimental effects and theoretical questions, has been extensively investigated.[2,5,6,8] Although some debate still remains, a large value for the VBO is now generally accepted. The band structure in the direction perpendicular to the superlattice growth also has important effects, especially with regard to transport properties, and has been investigated thoroughly.[2,6,9]

Various optoelectronic applications may require further knowledge of accurate wave functions: the primary purpose of this work is to advance this type of study. Our approach is based on a semiempirical TB model which includes fairly well all the important features of the band structures of the composing materials, and then uses a powerful renormalization technique[10] to determine both the band structure and the corresponding wave functions.

We begin our analysis (Sec. II) by considering a simple analytical continuum model, which reveals the peculiar occurrence and structure of interface states, caused by the coupling of effective masses with different signs. Then we introduce our microscopic approach (Sec. III), where the large rank of the TB Hamiltonian matrix is reduced systematically by a renormalization procedure. We also apply a modified Lanczos method to determine the orbital components of specific wave-function amplitudes. Applications to quantum wells (QW's) and SL's (Sec. IV) demonstrate a qualitative consistency with some features of the analytical model, but produce significantly more accurate results. In particular, the square magnitude of the different components of the interface wave functions on the various atomic orbitals of the basis set reveal the *s*-*p* hybridization associated with the mixing between Γ_6- and Γ_8-derived bands.

II. CONTINUUM MODEL AND GENERAL FEATURES OF THE INTERFACIAL STATES IN QUANTUM WELLS

The simplest method to study the qualitative features of the electronic structure of a quantum well is to solve a single-particle one-dimensional Schrödinger equation[11]

$$\left[-\frac{d}{dz}\left(\frac{\hbar^2}{2m^\star(z)}\frac{d}{dz}\right)+V(z)\right]\Psi(z)=\varepsilon\Psi(z), \tag{1}$$

with an effective mass $m^\star(z)$ that generally differs in the well and barrier. Boundary conditions at the interfaces are then imposed, requiring continuity of the wave function and current

$$\Psi(z)\big|_{-(L/2)-\delta}=\Psi(z)\big|_{-(L/2)+\delta}, \tag{2a}$$

$$\Psi(z)\big|_{(L/2)-\delta}=\Psi(z)\big|_{(L/2)+\delta},$$

$$\frac{1}{m^\star(z)}\frac{d\Psi(z)}{dz}\bigg|_{-(L/2)-\delta}=\frac{1}{m^\star(z)}\frac{d\Psi(z)}{dz}\bigg|_{-(L/2)+\delta}, \tag{2b}$$

$$\frac{1}{m^\star(z)}\frac{d\Psi(z)}{dz}\bigg|_{(L/2)-\delta}=\frac{1}{m^\star(z)}\frac{d\Psi(z)}{dz}\bigg|_{(L/2)+\delta}.$$

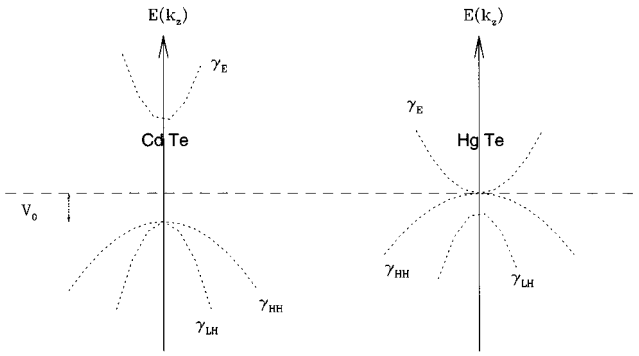

FIG. 1. Sketch of the band structure of CdTe and HgTe crystals, showing the bands deriving from Γ_8 and Γ_6 at the Brillouin-zone center. The effective masses corresponding to the Γ_8 coupling are indicated as γ_{LH} in CdTe, γ_E in HgTe, and γ_{HH} for heavy holes in both materials. The effective masses corresponding to the Γ_6 coupling are indicated as γ_E in CdTe and γ_{LH} in HgTe. The wave vector $\mathbf{k}$ is in the Γ-X direction, and V_0 is the valence-band offset between the two materials.

Stepwise potentials $V(z)$ can be chosen to represent different junction profiles. The current continuity, Eq. (2b), allows for interactions between states whose effective masses differ both in magnitude and sign.

The solution of Eqs. (2a) and (2b) is a linear combination of exponentials $e^{\pm\beta z}$ for $|z|\leqslant L/2$, and $e^{-\alpha|z|}$ for $|z|>L/2$. In the well, which we may, for example, associate with HgTe, $\beta=(1/\hbar)\sqrt{-2m_e\gamma_W(\varepsilon-V_1)}$ can be either real or purely imaginary. In the barrier, which we may correspondingly associate with CdTe, we always consider $\alpha=(1/\hbar)\sqrt{-2m_e\gamma_B(\varepsilon-V_0)}$ to be real: $\varepsilon>V_0$ if $\gamma_B<0$, or $\varepsilon<V_0$ if $\gamma_B>0$, where V_0 is the barrier height. We denote by γ effective masses in units of the electronic mass m_e.

In order to apply this analytical model, introduced originally by Ben Daniel and Duke,[12] we must consider the symmetry of the bands of the two semiconductors that interact in the microstructure. In a HgTe-CdTe heterojunction, we have basically three types of coupling around the fundamental energy gap: two are between Γ_8-type bands, and one is between Γ_6-type bands. For convenience, the basic band structure of the bulk materials around the Brillouin-zone center is sketched in Fig. 1. We may at first treat these couplings independently of each other. We may further assume that in the neighborhood of the Γ point each band is parabolic, so that an effective-mass description is justified. The corresponding values of $m^\star$ are then obtained from the Luttinger parameters introduced to describe the bulk materials.

Now, one Γ_8 coupling occurs between heavy holes, with $\gamma_{\mathrm{HH}}(\mathrm{CdTe})=-0.512$ and $\gamma_{\mathrm{HH}}(\mathrm{HgTe})=-0.588$. This produces a standard QW structure. The other Γ_8 coupling derives from the interaction between a light hole in CdTe, with $\gamma_{\mathrm{LH}}(\mathrm{CdTe})=-0.101$, and an electron in HgTe, with $\gamma_E(\mathrm{HgTe})=+0.027$. In this coupling, the effective masses differ in sign, hence both α and β are real and positive for energies such that $V_0<\varepsilon<0$, where $V_0=-0.450$ eV is the VBO that we assume, and the energy origin is set at the top of the HgTe valence band (hence $V_1=0$). So, only one state, and possibly a second one, can appear in this energy region, namely, a symmetric and an antisymmetric linear combina-

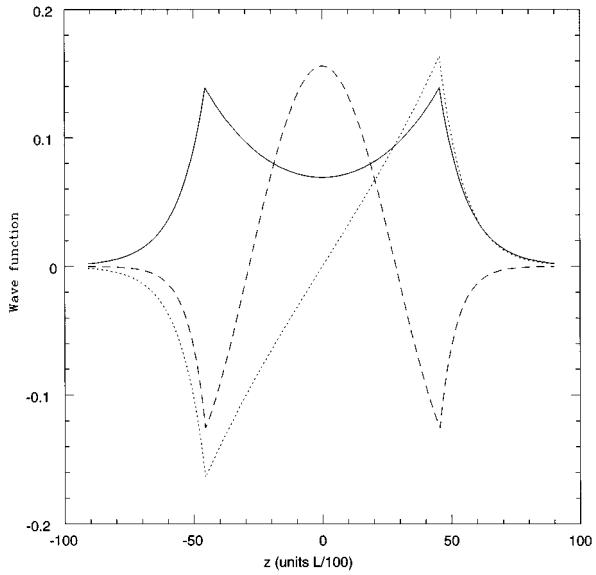

FIG. 2. Wave functions of the interfacial states $I1$ (solid line), $I2$ (dotted line), and $E3$ (dashed line) in a quantum well (QW) with $L=28\ (a/2)=90.3$ Å, calculated with the analytical model. Notice the derivative discontinuities at the interfaces, the shapes in the well (cosh-, sinh-, and cos-like), and the increasing number of nodes (none, one, and two).

tion of real exponentials, which we label in this paper as $I1$ and $I2$. The corresponding wave functions exhibit a discontinuity in the first derivatives at the interfaces, and have no node and one node, respectively. For positive energies, $\varepsilon>0$, we still have interfacial states with first-derivative discontinuities, although the exponentials are oscillatory in the well, since β is purely imaginary: we label this series of levels as $E2,E3,\ldots$. The wave functions of the three lowest interfacial states $I1$, $I2$, and $E3$ in the continuum model are shown in Fig. 2.

The dependence of the energy of the interfacial states on the width L of the well is easily determined by solving the transcendental equation which is derived from setting to zero the determinant of Eqs. (2), namely,

$$\frac{(\alpha\gamma_W-\beta\gamma_B)^2}{(\alpha\gamma_W+\beta\gamma_B)^2}=e^{2\beta L}. \tag{3}$$

If $\gamma_B<0$, the right-hand side of Eq. (3) diverges for an infinite well width. Correspondingly, the left-hand side diverges for

$$E^\star=\frac{V_0}{1+\dfrac{|\gamma_B|}{\gamma_W}}, \tag{4}$$

representing the asymptotic energy to which both $I1$ and $I2$ converge for an infinite well width. The energy of the confined symmetric (antisymmetric) state $I1(I2)$ is always below (above) $E^\star$.

Therefore, while $I1$ always exists, $I2$ actually becomes $E2$, corresponding to a purely imaginary β, if its energy becomes positive. Correspondingly, the wave-function second derivatives at each interface have opposite signs for an $E2$ state, whereas they have the same sign for an $I2$ state. Expanding Eq. (3) in the neighborhood of $\varepsilon\simeq 0$, we obtain the value of L at which the transition from positive energy, at shorter L, to negative energy, at larger L, occurs for the $E2/I2$ state:

$$L^\star=\frac{2|\gamma_B|}{\gamma_W}\left(\frac{\hbar^2}{2m_e|\gamma_B|(-V_0)}\right)^{1/2}. \tag{5}$$

For the effective masses reported above, we have $E^\star=-0.095$ eV and $L^\star=69$ Å$\simeq 21\,(a/2)$, a being the lattice constant. Notice that, since orthogonality and the inversion symmetry of this model Hamiltonian do not allow for more than two confined states with negative energies (and real-exponential wave functions), the energy of the $E3$ state must always be positive, and approaches zero with increasing L.

We notice at this point that we can also consider a CdTe well between two HgTe barriers. The mass signs are inverted with respect to the situation considered in the example above (of a HgTe well between two CdTe barriers). Consequently, the energy ordering of the interfacial states is also inverted, namely, $I1>I2/E2>E3>\ldots$, with the corresponding wave functions still exhibiting zero, one, two, ... nodes. Now, the magnitude of the ratio of the masses in the well and barriers is also inverted for the ''inverted'' series, which results in a greater wave-function penetration into the barriers. On the other hand, the asymptotic energy $E^\star$ remains the same in value for both the ''normal'' and ''inverted'' series, since it obviously coincides with the energy for a single interface.[13]

When we consider a SL, the transcendental equation corresponding to Eq. (3) is slightly more complicated. States with the same symmetry, i.e., an equal number of nodes, from the ''normal'' and the ''inverted'' QW series mix, while the levels also broaden into bands. In the limit of small band dispersion, one has the approximate energy relation

$$\epsilon(I1)\approx\epsilon_n(I1)+\epsilon_i(I1)-E^\star, \tag{6}$$

where the n and i subscripts refer to the ''normal'' and ''inverted'' series in the respective QW's. The same relation also holds for the $I2$ level. Then the ordering of the two levels in the SL is ''normal'' or ''inverted,'' depending on which of the corresponding two QW series has its levels further apart from $E^\star$. Because of the different wave-function penetrations, the ''normal'' series ordering usually prevails in SL's. But, for increasingly small CdTe slabs, there is eventually an (anti)crossing, whereby the $I2$-derived level descends below the $I1$-derived level, producing an ''inverted'' ordering in the SL. In all cases, an energy gap (direct or inverted) exists between the $I1$- and $I2$-derived bands in the SL. With regard to $E3,E4,\ldots$ levels, they form bands in the SL, above (below) the top of the HgTe (CdTe) valence band, mostly derived from the ''normal'' (''inverted'') QW series.

Interface states also originate from the coupling between electron states in CdTe and light-hole states in HgTe, both with Γ_6 symmetry, since a change in the sign of the effective masses also occurs: $\gamma_E(\mathrm{CdTe})=+0.099$, and $\gamma_{\mathrm{LH}}(\mathrm{HgTe})=-0.031$. With respect to the previous case of the Γ_8 coupling, since the mass signs are opposite, the ordering of the energy levels is reverted. A larger barrier height

also occurs. Since we need to retain the same energy origin at the top of the HgTe valence band, we now have to set for the ''normal'' series the bottom of the HgTe well at $V_1=-0.303$ eV, and $V_0=+1.13$ eV in the CdTe barrier. The asymptotic energy and the $E2/I2$ transition width predicted by the continuum model are in this case $E^\star=0.041$ eV and $L^\star\simeq 33$ Å$\simeq 10(a/2)$. Once again, we also have an ''inverted'' series, corresponding to a CdTe QW , with an energy ordering that is then the same as that of the ''normal'' series for the HgTe well and the Γ_8 coupling. The same considerations about the asymptotic energy and the mixing when SL's are considered of course apply to both couplings, separately.

As we have already noticed, the coupling between heavy holes of Γ_8 symmetry in both CdTe and HgTe leads to the standard QW level quantization, since the effective masses have the same (negative) sign in both the barrier and well. Consequently, one obtains a rather complex behavior of the energy gap in microstructures of varying L, because of various crossings between interface and heavy-holes states.

The basic trends predicted by the continuum model are confirmed by the microscopic investigation that we describe in the following sections, but apparently with restriction to Γ_8 coupling. In fact, only the microscopic investigation can fully demonstrate the structure induced by the Γ_8-Γ_6 mixing.

III. RENORMALIZATION AND MODIFIED LANCZOS METHODS

In order to obtain quantitative results for QW's and SL's of HgTe-CdTe, it is necessary to consider from the start the entire band structure of the composing materials, which includes not only the peculiar effects due to the change of sign in the effective masses, but also the effects of nonparabolicity and warping occurring away from the Γ point. These can be included by introducing a semiempirical TB parametrization of the bulk materials. In this work, we use a $sp^3s^\star$ basis set of the type introduced by Dow and co-workers.[14] The optimization of our TB parametrization to describe best the QW and SL states in the energy range of interest is discussed in the Appendix.

We should note that the strain caused by the small lattice mismatch between the HgTe and CdTe lattice constants may produce some important effects in the heterostructures, exchanging the order of some levels.[4,5] However, the effect on the wave functions is less significant, and will be ignored in this work.

The dimension N of the TB Hamiltonian matrix is given by the number of basis atomic orbitals per atom (which is ten here, including spin) times the number of atomic planes in the microstructure supercell. Such a dimension becomes quite large for thick SL's. However, this poses no problem and can be handled very efficiently with a renormalization procedure based on the Green's function and a systematic reduction of degrees of freedom. Expanding the Hamiltonian on the basis of two-dimensional Bloch sums, and considering (for the sake of simplicity) only nearest-neighbor interactions, one starts from a block-tridiagonal matrix, representing the system as a linear chain. To that, one applies recursively the decimation formulas

$$H_1^R=H_1+C_{12}\frac{1}{\epsilon-H_2}C_{21}, \tag{7}$$

$$C_{13}^R=C_{12}\frac{1}{\epsilon-H_2}C_{23}, \tag{8}$$

yielding the on-site and first-neighbor renormalized interactions.[10] For the given TB parametrization, the renormalization procedure requires inversion and processing only of small (10×10) matrices. The eigenvalues are obtained as poles of the Green's function. The computational time involved in the whole process scales as $\log_2 N$.

This method has consistently proved to be extremely effective in determining the full energy spectrum in various systems.[15,16] On the other hand, it provides directly only the square magnitude of the wave-function weight on any given atomic orbital and site, as residue at the pole of the Green's-function matrix element on that atomic orbital and site. Thus, we have also calculated the wave-function *amplitude*, using an alternative modified two-step Lanczos method,[17] which proceeds as follows. The original Hamiltonian is used to derive an auxiliary operator $A=(H-\epsilon)^2$, where ϵ can be chosen as an eigenvalue obtained by the renormalization method. In this case, A has a ground-state zero eigenvalue, and an appropriate minimization procedure allows us to determine the corresponding eigenvector as follows. Starting from an arbitrary vector $|f_0\rangle$, we obtain

$$|F_1\rangle=A|f_0\rangle-a_0|f_0\rangle, \tag{9}$$

where $a_0=\langle f_0|A|f_0\rangle$. Then we normalize $|F_1\rangle=|F_1\rangle/b_1$, where $b_1^2=\langle F_1|F_1\rangle$, and $a_1=\langle F_1|A|F_1\rangle$ is calculated. Diagonalization of

$$M=\begin{pmatrix} a_0 & b_1 \\ b_1 & a_1 \end{pmatrix} \tag{10}$$

produces a new vector $|F_2\rangle=c_1|f_0\rangle+c_2|F_1\rangle$, corresponding to the smallest eigenvalue of M. After normalization, $|F_2\rangle$ can be used as $|f_0\rangle$, to restart the process. Convergence can be accelerated by appropriately introducing at some point an n step $(n\geqslant 2)$ Lanczos procedure.[18] Eventually, the complete eigenfunction for the eigenvalue ϵ is thus obtained.

IV. HETEROSTRUCTURES OF HGTE-CDTE

A. Quantum wells

The phenomenology described in Sec. II with the continuum model can now be analyzed much more accurately with the microscopic TB-renormalization scheme. We have calculated the energy levels for many different well widths, and then identified the interfacial and heavy-hole states by inspection of the square magnitudes of the corresponding wave functions. The shapes of the wave functions reveal clearly the types of states that are involved. In case of any doubt, the modified Lanczos method can further provide the detailed nodal structure of all the amplitude components.

First of all, we note that there are no states in the explored energy region (between -1 and 1 eV) which correspond to those predicted by the continuum model for the Γ_6 coupling *separately*. This is probably due to the actual shape of the

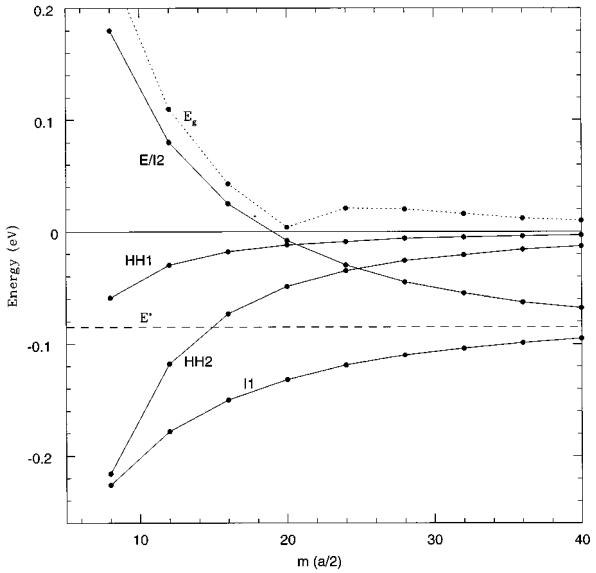

FIG. 3. Energies of heavy holes confined states (HH1, HH2) and interfacial states ($I1$,$E2/I2$) vs well width in multiple QW's of $(HgTe)_m(CdTe)_{40}$, with $m=8,12,\ldots,36,40$, in $a/2$ units. Because of the thickness of the CdTe barrier, no tunneling and/or dispersion can occur. The peculiar confinement of $I1$ and $E2/I2$ states with respect to the asymptotic energy $E^\star$, combined with the standard heavy-hole confinement, nearly cause the annihilation of the gap (E_g) at a single-well width. These microscopic results match closely those of the analytical model.

Γ_6 band in HgTe, which exhibits a strong nonparabolicity, and can only be included correctly by the microscopic TB parametrization.

On the other hand, the energy trend of $I1$ and $I2$ states vs well width L permits us to extrapolate the asymptotic energy of the Γ_8 coupling as $E^\star=-0.085$ eV, and the critical width for the $E2/I2$ transition as $L^\star=18(a/2)$, which agree surprisingly well with the predictions of the continuum model: see Fig. 3. The energy gap evolution depends on the relative position between occupied and unoccupied states, i.e., $E_g=|\varepsilon(E2/I2)-\varepsilon(\mathrm{HH1})|$ if $\varepsilon(E2/I2)\geqslant\varepsilon(\mathrm{HH2})$, and $E_g=\varepsilon(\mathrm{HH1})-\varepsilon(\mathrm{HH2})$ if $\varepsilon(E2/I2)\leqslant\varepsilon(\mathrm{HH2})$. This of course applies to multiple QW's, for which the wide barrier in the supercell forbids any tunneling and dispersion in the k_z direction for any energy level, hence any semimetallic region in a finite range of well widths.

We show in Figs. 4–7 the square magnitude of some wave functions in a HgTe multiple QW, calculated microscopically with the renormalization method. These wave functions exhibit some features that are typical of the analytical model, although the relative weights of different orbital components and anion vs cation localization are clearly beyond that. As expected, the HH states are almost completely (p_x,p_y)-like, whereas interface states show a considerable mixing between s and p orbitals. Because of that, the shape of the corresponding microscopic wave functions can be very different from those of the continuum model, particularly on the cation sites: compare Figs. 6(b) and 7(b) for the microscopic $I2$ and $E3$ states with Fig. 2 for the continuum model. Such an effect undoubtedly originates from the mixing of particular bulk material band structures, as will be further illustrated and clarified in the SL structures that we discuss next.

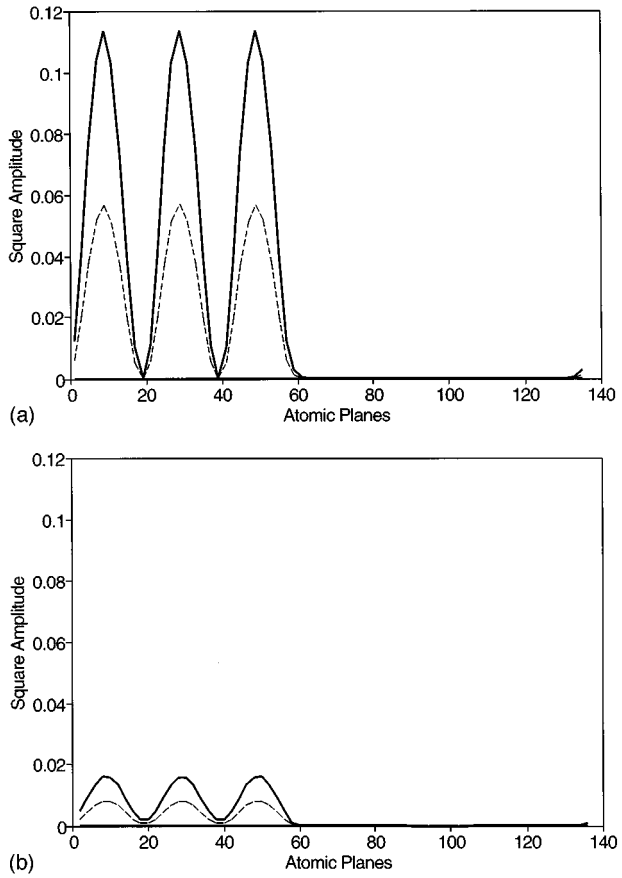

FIG. 4. Square magnitude of the wave-function coefficients on the atomic orbitals used in the localized orthonormal basis set, for a $(HgTe)_{28}(CdTe)_{40}$ multiple QW, on the anion (a) and cation (b) sites. We show the total square magnitude of the HH3 wave function on different sites (thick solid line), the weights of the degenerate p_x and p_y components (dashed line), the weight of the p_z component (solid line), and the weight of the s component (dotted line). Evidently, the heavy-hole states are almost exclusively (p_x,p_y) like, with the standard nodal structure.

B. Superlattices

The general features of the electronic structure in SL's grown in the [001] direction are similar to those in QW's, although the effect of the energy dispersion in the k_z direction becomes crucial, causing a semimetallic behavior in a certain range of well widths.[2,6] We have verified that this is due to the (anti)crossing with the HH1 band of the $I2$ broadband, as it descends in energy with increasing well width (toward an asymptotic energy). The corresponding band structure also allows us to determine the changes in the carrier effective masses in the k_z direction. The in-plane band dispersion must be further explored to determine whether or not additional crossings may occur.[5,9] Our calculations indicate that this does not happen, since at $\mathbf{k}=0$ the conduction band has a positive curvature in any direction. All these results are consistent with the previous literature on this problem, and will not be discussed further here.

The focus of this work is to analyze the interfacial wave functions of [001] SL's, which depend crucially on the Γ_6-Γ_8 band mixing. To demonstrate that, with only a few examples, we choose to discuss in particular only the results

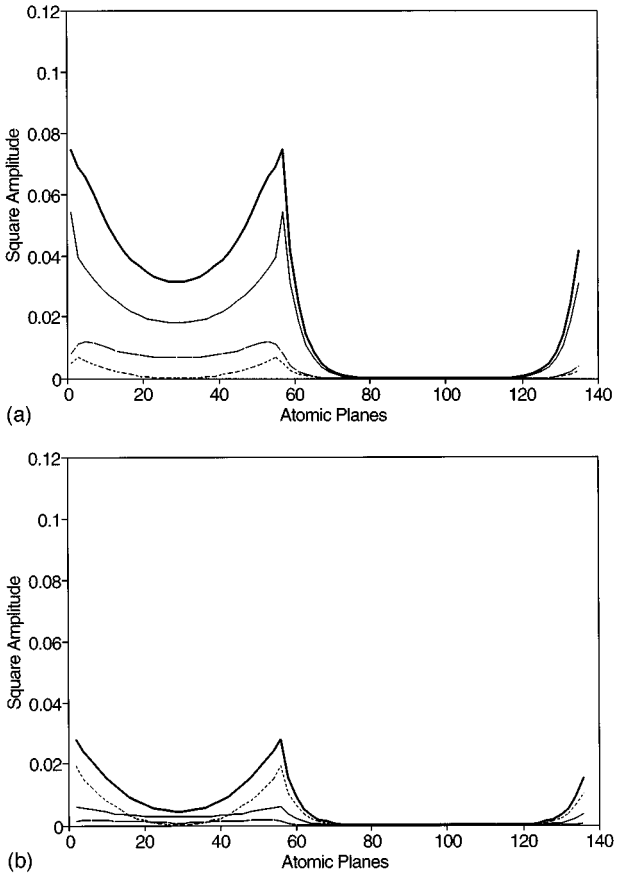

FIG. 5. For the same multiple QW and with the same notations as in Fig. 4, we now show the interfacial $I1$ wave function. Notice that it has no nodes in the p components, as predicted by the analytical model for Γ_8 coupling. But beyond that, it also has an s component with one node.

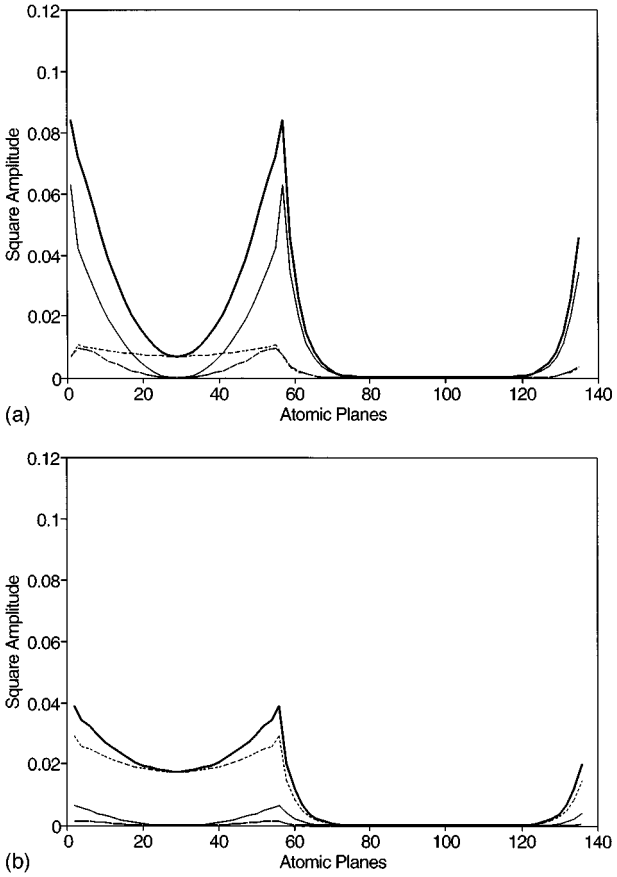

FIG. 6. Same as Fig. 5, but for the $I2$ state. Now the p components have one node, as predicted by the analytical model for Γ_8 coupling, while the s component has no nodes.

for relatively thin superlattices $(HgTe)_{16}(Hg_{1-x}Cd_xTe)_8$, where the barrier is progressively built up from the folded HgTe band structure, by alloying it with an increasing Cd concentration x (the virtual-crystal approximation is used for that). Adding Cd in the barrier has the simultaneous effect of generating a confinement, due to the increase of a VBO equal to $(-0.450)x$, and a perturbation, due to the change in the barrier composition. One can distinguish between these two effects by comparing the results with those having the VBO artificially kept at zero, or with those having an imposed stepwise potential on the folded band structure of pure HgTe.

The results show, first of all, that the HH bands are the least affected by the Cd and VBO introduction, except for standard confinement. This agrees with the almost exclusive (p_x,p_y) composition of HH wave functions, at all Cd concentrations. More interestingly, the first folded Γ_6 band of HgTe goes up quickly as the Cd concentration in the barrier increases up to a critical $x_c=0.55$, where it (anti)crosses and rises to become the $I2$-derived band of the $(HgTe)_{16}(CdTe)_8$ SL: see Fig. 8. The existence of such an interface state is also predicted by the analytical model, resulting, however, only from the Γ_8 coupling. On the other hand, the second folded Γ_6 band of HgTe hardly moves as the Cd concentration in the barrier increases (this band is lower in energy, and is not shown in Fig. 8).

Now the composition of the Γ_6 band in HgTe is of s type, and at low x its first folding generates an interfacial state (at the SL $\mathbf{k}=0$) of $I1$ type, essentially derived from the ''inverted'' series of Γ_6 coupling in the alloy SL. When more Cd is added in the barrier, small projections on the p_z states [and even smaller (p_x,p_y) projections] appear at both anion and cation sites, corresponding to the $I2$ wave function derived from the ''inverted'' series of the Γ_8 coupling. Because of the Γ_8 coupling, we call such a SL band $I2$ derived, for all values of x. The p components become greater and greater (see Fig. 9), until the critical concentration $x_c=0.55$ is reached. After that, the wave function does not qualitatively change.

We can similarly analyze the other interfacial state. Starting from the folded Γ_8 band of HgTe, which is of p type, the $I1$ band immerses into the SL valence bands (because of the confinement induced by the increasing VBO), (anti)crossing the HH1 band (which is nearly flat in the k_z direction), and then the HH2 band. At the critical concentration x_c, it (anti)crosses the $I2$ band discussed above, and further descends to become the $I1$-derived band of the pure $(HgTe)_{16}(CdTe)_8$ SL: see Fig. 8. The corresponding wave function is essentially derived at small x from the $I1$ state of the ''inverted'' series of the Γ_8 coupling. Because of the Γ_8 coupling, we consistently call such a SL band $I1$ derived,

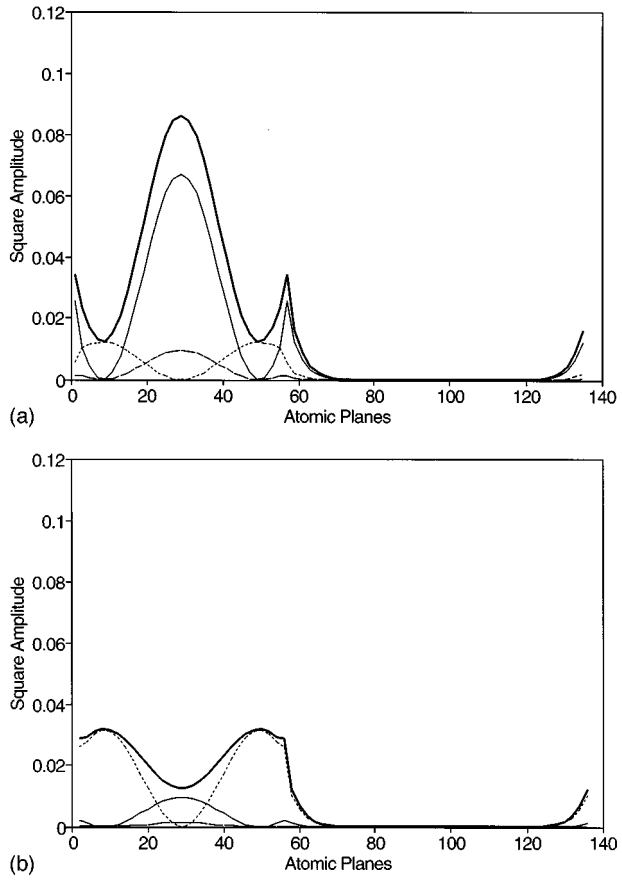

FIG. 7. Same as Figs. 5 and 6, but for the $E3$ state. Notice that the p_z component, with two nodes, tends to prevail on the anions, whereas the s component, with one node, tends to prevail on the cations, which results in an almost opposite localization of the total wave function on the two types of sites.

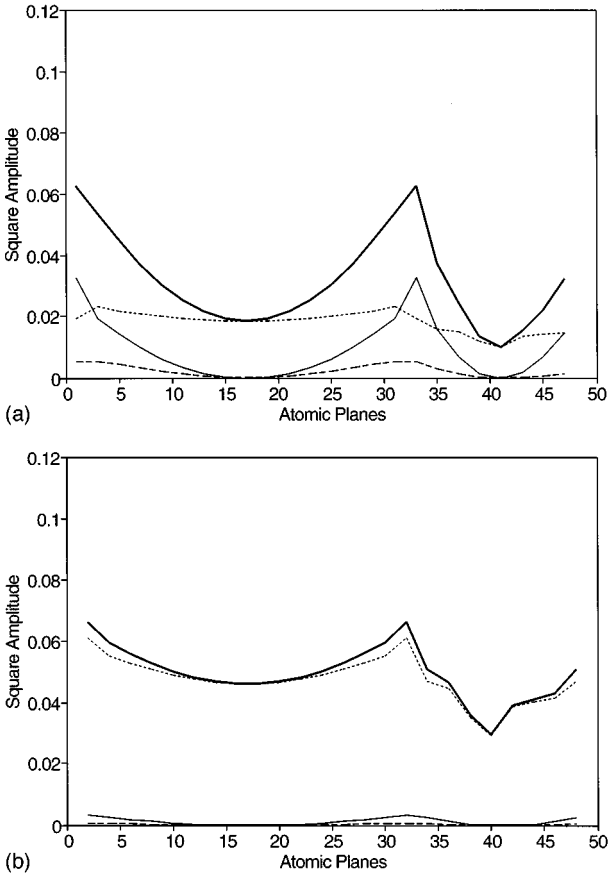

FIG. 9. Square magnitude of the $I2$-derived wave function (at the SL $\mathbf{k}=0$) of $(HgTe)_{16}(Hg_{1-x}Cd_xTe)_8$ with $x=0.5$, slightly below the critical concentration $x_c=0.55$. The wave function is concentrated more on the cations. Compare with Fig. 6 for a multiple QW.

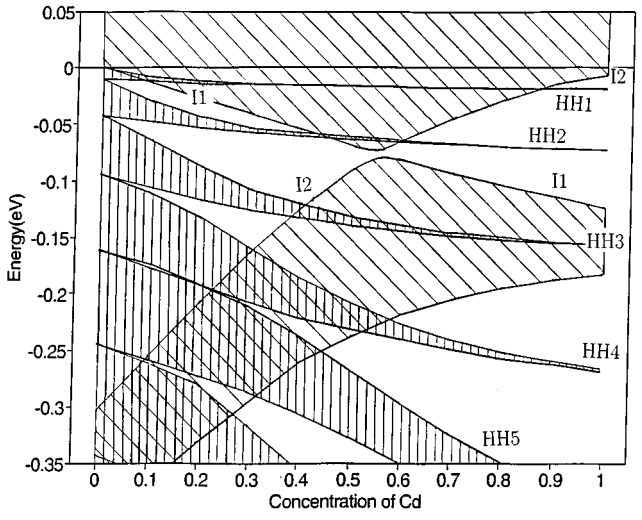

FIG. 8. Projected bands (in the k_z direction) vs increasing Cd concentration in the barrier for $(HgTe)_{16}(Hg_{1-x}Cd_xTe)_8$ SL's. The combined effect of increasing VBO and alloy perturbation on the folded HgTe band structure opens gaps and flattens the HH bands, narrowing their projection. Interfacial bands (anti)cross at a critical concentration $x_c \simeq 0.55$, an effect related to the band inversion occurring in the simple alloy.

for all values of x. With increasing Cd concentration, the wave function does not change qualitatively, although a small s-component appears, signaling mixing with $I2$ of the ''normal'' series for the Γ_6 coupling. Approaching the critical concentration, a peculiar influence from the $I2$-derived state appears at $x=0.5$, where the p components of the $I1$-derived state ''attempt'' to form a node as well: see Fig. 10. After x_c, the typical $I1$ mixed structure is resumed in the wave function, up to $x=1$ of the pure SL. Quite clearly, the behavior of the $I2$- and $I1$-derived wave functions are orthogonal and complementary to each other (including their larger localization on the cation and anion sites, respectively).

Evidently, the critical concentration corresponds to the point of maximal Γ_6-Γ_8 band mixing in the SL, which is further confirmed by the analysis of other interfacial states. Interestingly, this critical concentration x_c is directly related to the transition from semimetal to semiconductor in the $Hg_{1-x}Cd_xTe$ simple alloy, occurring at a concentration x_a about one-third of x_c, for which the relative weight of Cd in the whole SL is precisely the same as in the alloy.

We now study the $E3$-derived level at positive energies. As expected, it approaches the zero of energy as the well width is increased. This excludes additional crossings with the HH1 band, and hence additional semiconductor-

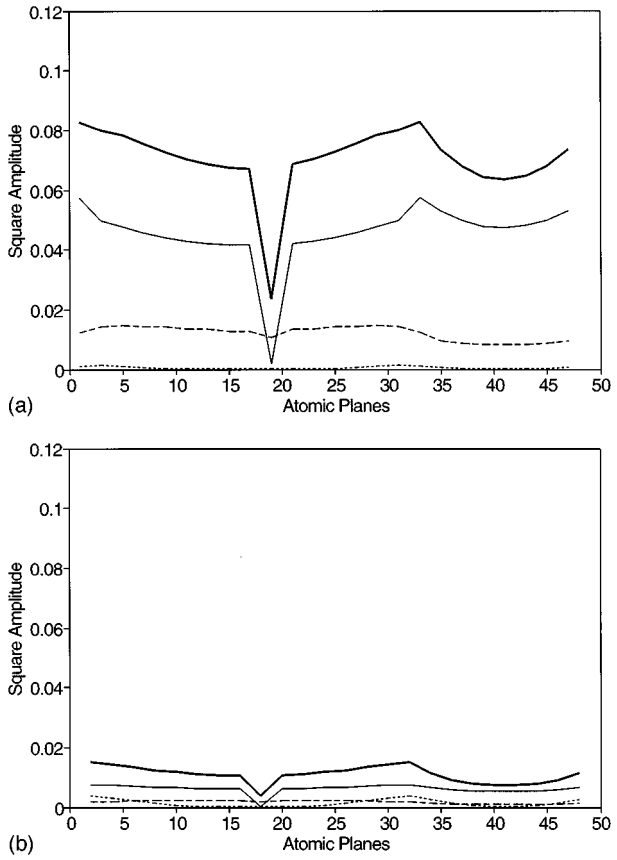

FIG. 10. Square magnitude of the $I1$-derived wave function of $(HgTe)_{16}(Hg_{1-x}Cd_xTe)_8$ for $x=0.5$, showing that the p components ''attempt'' to form a node, due to the influence of the $I2$-derived state. The localization is larger on the anions, and the components are largely p like. Compare with Fig. 5 for a multiple QW.

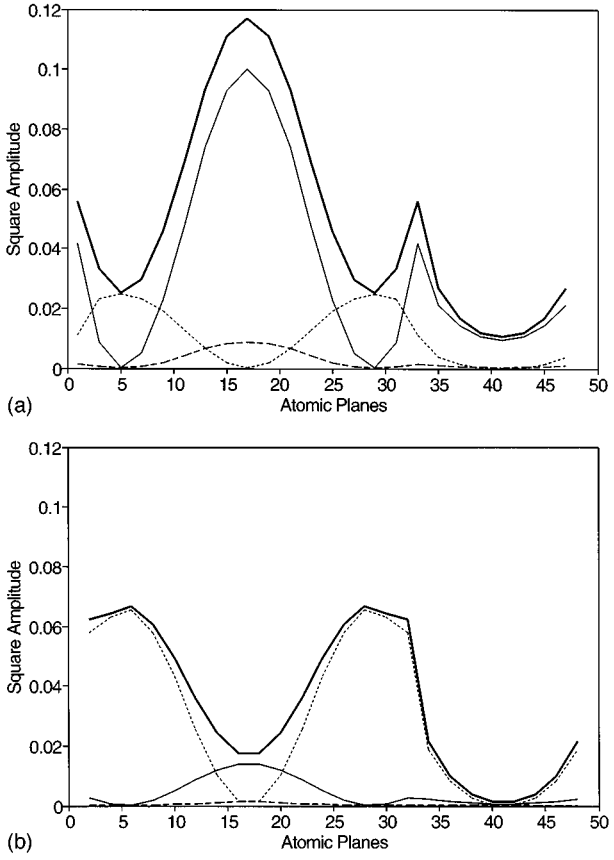

FIG. 11. Square magnitude of the $E3$ wave function of $(HgTe)_{16}(CdTe)_8$, showing the nodal structure for s and p components, which also have different weights on anions (a) and cations (b). Compare with Fig. 7 for a multiple QW.

semimetal transitions. With regard to the dependence on the Cd concentration x in the barrier, the only effect is a considerable reduction of the dispersion (in the k_z direction), due to the localizing effect of the VBO with increasing x. The $E3$ wave function has orbital s and p components having one and two nodes, respectively (see Fig. 11), for the pure SL. The p_z-orbital content is greater on anion sites, while the s-orbital content is prevalent on cation sites. Around the critical concentration x_c, the expected discontinuity of the first derivative at the interface becomes more evident, but without any abrupt transition. To obtain the precise nodal structure of each orbital amplitude, hence that of the total wave function, one can use the modified Lanczos method. In Fig. 12, we show the complete wave-function *amplitude* components for such an $E3$ state. Continuing this analysis, the En-derived states with higher energies show a predictable structure, with s and p components exhibiting $n-2$ and $n-1$ nodes, respectively.

C. Considerations on the VBO

The problem of the VBO has been extensively investigated by many authors.[2,6,8] In this section, we briefly report our results on this question. We have considered different VBO values, ranging from 0.0 to -0.450 eV, and examined the corresponding confining effect on the various types of bands.

In quantum wells, the HH states, once confined, hardly change with increasing VBO, as expected. On the other

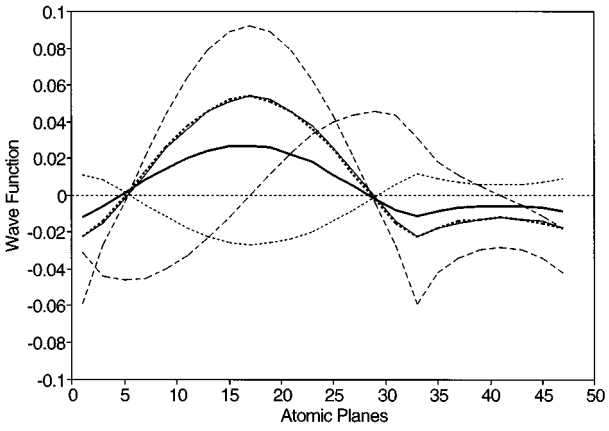

FIG. 12. Real and imaginary parts of s, p_x, p_y, and p_z components of the wave-function amplitude of the $E3$ state corresponding to Fig. 11(a), calculated by the modified Lanczos method. Re$[s]$ and Re$[p_z]$ are essentially zero. Re$[p_x]$: heavy solid. Re$[p_y]$: heavy dotted. Im$[s]$: dash-dotted. Im$[p_x]$: solid. Im$[p_y]$: dotted. Im$[p_z]$: dash. Notice again that the s (p) components have one (two) node(s).

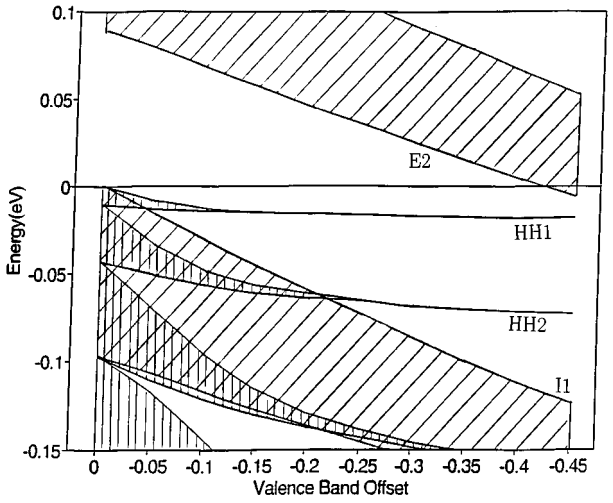

FIG. 13. Projected band structure in the k_z direction for $(HgTe)_{16}(CdTe)_8$ SL with a VBO varying from 0.0 to -0.45 eV. Notice the different effect of the VBO on HH bands and interfacial $(I1,E2/I2)$ bands.

hand, the interface states $I1$ and $I2$ considerably descend in energy (by about 90 meV) with increasing VBO. Such a decrease of the $I1$ and $E2$ energies is essentially linear in the VBO, and can be associated with the descent of the asymptotic energy $E^{\star}$, which is indeed proportional to the VBO in the analytical model.

In SL's, a wide gap on the folded Γ_6 band of HgTe is introduced by alloying with Cd the barrier, even if we artificially maintain a zero VBO. On the other hand, the effect of the VBO on the $I1$ and $E2/I2$ bands (broadened by the dispersion in the k_z direction) is analogous to that in QW's. In Fig. 13 we show such dependence. We remark that a small (large) VBO implies a higher (lower) $E2/I2$ energy, hence a larger (smaller) HgTe well width L is required to attain the semiconductor $\rightarrow$ semimetal transition. In $(HgTe)_m(CdTe)_8$, for a VBO equal to -0.040 eV we obtain $L \simeq 30(a/2)$, i.e., $m=30$, whereas for a VBO equal to -0.450 eV, we obtain $L \simeq 20(a/2)$. By comparing with experimental data, this may be used as a criterion to further investigate the small vs large VBO issue in these heterostructures.

V. CONCLUSIONS

We have calculated the electronic states, and analyzed in detail the corresponding wave functions in HgTe-CdTe quantum wells and superlattices. This has advanced a quantitative understanding of the s-p mixing in the interfacial states resulting from the inverted band structure of HgTe. A simple analytical continuum model has proved useful in interpreting some basic features of such states, but is unable to account quantitatively for the Γ_6 coupling, and even qualitatively for the s-p mixing. Our microscopic study is based on a tight-binding Hamiltonian, with parameters optimized so as to reproduce reliably the overall band dispersion in the Brillouin zones of the composing materials, while retaining the needed accuracy for the effective-mass tensors near the zone centers. Our method of solution is based on the Green's function and the renormalization-decimation procedure. That requires an inversion only of small matrices of fixed rank, which becomes crucial for large supercells, since the computation scales only logarithmically with the supercell dimension. The weight of the wave-function components on all the atomic sites and orbitals in the basis are accurately determined as residues at the poles of the corresponding Green's-function matrix elements. Even the wave-function *amplitude* can be determined accurately by an alternative modified (two- or n-step) Lanczos method. The knowledge of accurate wave-function amplitudes is clearly essential for further studies of both direct optical transitions and indirect transitions assisted by interface phonons.[19]

TABLE I. Tight-binding parameters.

	CdTe	HgTe
$E_{s,a}$	-8.192	-8.072
$E_{p,a}$	0.328	0.448
$E_{s,c}$	-0.950	-3.521
$E_{p,c}$	6.938	5.058
$E_{s*,a}$	10.445	3.656
$E_{s*,c}$	6.630	9.427
$4E_{s,s}$	-5.0	-5.0
$4E_{x,x}$	2.136	2.056
$4E_{x,y}$	5.081	4.189
$4E_{s,p}$	3.840	3.942
$4E_{p,s}$	5.883	5.522
$4E_{s*,p}$	4.373	3.769
$4E_{p,s*}$	3.699	5.649
Δ_a	0.968	1.03
Δ_c	0.227	0.86
γ_1	5.923	-17.872
γ_2	1.986	-9.786
γ_3	2.463	-9.345
m_c	0.099	-0.031
γ_1	4.110[a]	-18.680[b]
γ_2	1.080[a]	-10.190[b]
γ_3	1.950[a]	-9.560[b]
m_c	0.099[a]	-0.031[b]

[a]Reference 21.
[b]Reference 22.

ACKNOWLEDGMENTS

This work was supported in part by the U.S. Army Research Office under Contract No. DAAH04-93-G-0236 and in part by the Italian Istituto Nazionale di Fisica della Materia.

APPENDIX: TIGHT-BINDING PARAMETRIZATION OF THE BULK MATERIALS

In this appendix, we summarize the procedure that we developed to optimize the TB parameters describing the composing materials of the SL's. Essentially the same procedure was previously used in Ref. 16.

We start with the TB parameters of Schulman and Chang,[20] and then adjust their $E_{s,p}$ and $E_{p,s}$ to better reproduce the electron effective mass m_c, and their $E_{x,y}$ to better reproduce the heavy-hole effective mass in the [001] direc-

tion. The latter is related to the Luttinger parameters as $1/m_{\mathrm{HH}}[001]=\gamma_1-2\gamma_2$. These parameters are very important in order to describe accurately QW and SL states in the energy region of interest, which is around the HgTe zero gap. At the same time, our parametrization procedure allows us to retain a good overall description of the bands of the composing materials in their entire Brillouin zone. We have assumed the values of m_c and γ_i given in Refs. 21 and 22, for CdTe and HgTe, respectively. These are reported in the last four lines in Table I. We then provide in Table I our adjusted parameters, using essentially the same notations as in the original Table I of Ref. 20. We also show the m_c and γ_i values that result from our optimization of the TB parameters (four lines above the last four of Table I).

We have also considered other sets of TB parameters, to test the dependence on those of the SL bands of interest. Although we found a certain dependence, the basic trends and ordering of the levels are always maintained. This is also consistent with the fact that the band structures that we obtain are generally in good agreement with those previously reported in the literature,[4,5] which are obtained by different methods and parametrizations.

[1] Y. Lansari, J. W. Han, S. Hwang, J. W. Cook, Jr., and J. F. Schetzina, J. Vac. Sci. Technol. A **7**, 241 (1989).

[2] Z. Yang, Z. Yu, Y. Lansari, S. Hwang, J. W. Cook, Jr., and J. F. Schetzina, Phys. Rev. B **49**, 8096 (1994).

[3] J. M. Perez, R. J. Wagner, J. R. Meyer, J. W. Han, J. W. Cook, Jr., and J. F. Schetzina, Phys. Rev. Lett. **61**, 2261 (1988); C. A. Hoffman, J. R. Meyer, F. J. Bartoli, J. W. Han, J. W. Cook, Jr., J. F. Schetzina, and J. N. Schulman, Phys. Rev. B **39**, 5208 (1989); M. Dobrowolska, T. Wojtowicz, H. Luo, J. K. Furdyna, O. K. Wu, J. N. Schulman, J. R. Meyer, C. A. Hoffman, and F. J. Bartoli, *ibid.* **41**, 5084 (1990); J. R. Meyer, R. J. Wagner, F. J. Bartoli, C. A. Hoffman, M. Dobrowolska, T. Wojtowicz, J. K. Furdyna, and L. R. Ram-Mohan, *ibid.* **42**, 9050 (1990).

[4] G. Bastard, C. Delalande, Y. Guldner, and P. Voisin, Adv. Electron. Phys. **72**, 1 (1988); L. R. Ram-Mohan, K. H. Yoo, and R. L. Aggarwal, Phys. Rev. B **38**, 6151 (1988); K. H. Yoo, R. L. Aggarwal, and L. R. Ram-Mohan, J. Vac. Sci. Technol. A **7**, 415 (1989); K. C. Hass and D. J. Kirill, Phys. Rev. B **42**, 7042 (1990).

[5] J. R. Meyer, F. J. Bartoli, C. A. Hoffman, and J. N. Schulman, Phys. Rev. B **38**, 12 457 (1988); C. A. Hoffman, J. R. Meyer, F. J. Bartoli, J. W. Han, J. W. Cook, Jr., J. F. Schetzina, and J. N. Schulman, *ibid.* **39**, 5208 (1989).

[6] N. F. Johnson, P. M. Hui, and H. Ehrenreich, Phys. Rev. Lett. **61**, 1993 (1988); P. M. Hui, H. Ehrenreich, and N. F. Johnson, J. Vac. Sci. Technol. A **7**, 424 (1989); C. A. Hoffman, J. R. Meyer, F. J. Bartoli, Y. Lansari, J. W. Cook, Jr., and J. F. Schetzina, Phys. Rev. B **40**, 3867 (1989); Z. Yang, Z. Yu, Y. Lansari, J. W. Cook, Jr., and J. F. Schetzina, J. Vac. Sci. Technol. B **9**, 1799 (1991).

[7] D. L. Smith, T. C. McGill, and J. N. Schulman, Appl. Phys. Lett. **43**, 180 (1983).

[8] J. M. Berroir, Y. Guldner, J. P. Vieren, M. Voos, X. Chu, and J. P. Faurie, Phys. Rev. Lett. **62**, 2024 (1989); J. B. Choi, L. Ghenim, R. Mani, H. D. Drew, K. H. Yoo, and J. T. Cheung, Phys. Rev. B **41**, 10 872 (1990); P. M. Young and H. Ehrenreich, *ibid.* **43**, 12 057 (1991); J. R. Meyer, C. A. Hoffman, R. J. Wagner, and F. J. Bartoli, *ibid.* **43**, 14 715 (1991).

[9] J. R. Meyer, D. J. Arnold, C. A. Hoffman, F. J. Bartoli, and L. R. Ram-Mohan, Phys. Rev. B **46**, 4139 (1992); J. R. Meyer, C. A. Hoffman, and F. J. Bartoli, Physica B **191**, 171 (1993).

[10] P. Giannozzi, G. Grosso, S. Moroni, and G. Pastori Parravicini, Appl. Numer. Math. **4**, 273 (1988).

[11] G. Bastard, Phys. Rev. B **25**, 7584 (1982); Y. Guldner, G. Bastard, and M. Voos, J. Appl. Phys. **57**, 1403 (1985); G. Bastard, *Wave Mechanics Applied to Semiconductor Heterostructures* (Les Editions de Physique, Les Ulis Cedex, 1989).

[12] D. J. Ben Daniel and C. B. Duke, Phys. Rev. **152**, 683 (1966).

[13] Yia-Chung Chang, J. N. Schulman, G. Bastard, Y. Guldner, and M. Voos, Phys. Rev. B **31**, 2557 (1985).

[14] P. Vogl, H. P. Hjalmarson, and J. D. Dow, J. Phys. Chem. Solids **44**, 365 (1983); A. Kobayashi, O. F. Sankey, and J. D. Dow, Phys. Rev. B **25**, 6367 (1982).

[15] R. D. Graft, G. Grosso, D. J. Lohrmann, L. Martinelli, S. Moroni, G. Pastori Parravicini, and L. Resca, in *Progress in Electron Properties of Solids*, edited by E. Doni, R. Girlanda, G. Pastori Parravicini, and A. Quattropani (Kluwer, Dordrecht, 1989), pp. 409–438.

[16] R. D. Graft, D. J. Lohrmann, G. Pastori Parravicini, and Lorenzo Resca, Phys. Rev. B **36**, 4782 (1987); G. Grosso, S. Moroni, and G. Pastori Parravicini, *ibid.* **40**, 12 328 (1989).

[17] G. Grosso, L. Martinelli, and G. Pastori Parravicini, Nuovo Cimento **15**, 269 (1993).

[18] G. Grosso, L. Martinelli, and G. Pastori Parravicini, Phys. Rev. B **51**, 13 033 (1995).

[19] M. Dutta and M. A. Stroscio, J. Appl. Phys. **73**, 1693 (1993); M. A. Stroscio, M. Dutta, and X. Q. Zhang, *ibid.* **75**, 1977 (1994).

[20] J. N. Schulman and Yia-Chung Chang, Phys. Rev. B **33**, 2594 (1986).

[21] Ch. Neumann, A. Nöthe, and N. O. Lipari, Phys. Rev. B **37**, 922 (1988).

[22] P. Lawaetz, Phys. Rev. B **4**, 3460 (1971).